A Migration Approach to Generating Continuous Images of Salt and Sediment Boundaries from Multi-Offset VSP Data

Jakob Haldorsen, Nicholas Brooks, READ AS; Pat Donais, Werner Heigl, Apache Corp; and Fred Li, Microview Technology Inc.

Abstract

We introduce a migration-based method for imaging the flank of a salt body providing a significant improvement compared to traditional methods. The method allows using a standard VSP array tool without rigid interconnects or gyroscope, as is required for conventional VSP salt proximity surveying.

The method come in two versions – one "heavy" and one "light" version – both using a version of reverse-time migration, applied to three-component borehole seismic data. The method allows the reconstruction of both the salt flank itself, and - using the light version - the sediments that juxtapose the salt body.

To demonstrate the methods, we have applied them to VSP data acquired along the Midway Dome, in Mississippi, USA.

Introduction

Salt-related structures are common in many areas in the world, amongst which is the US Gulf Coast region. Many conventional reservoirs are related to these structures as they create pathways and traps for hydrocarbons.

Salt domes and some isolated salt bodies often have steeply inclined and complex boundaries.

Steep boundaries are difficult to image directly with the surface-seismic method since reflections from these boundaries will tend to be down-going and will not be recorded with receivers at or near the surface. Such steep boundaries are commonly characterized by the absence of amplitude or termination of sub-horizontal features in images obtained from surface-seismic data. Figure 1 shows a schematic of a typical salt dome and related structures. Sedimentary layers are generally dragged upwards during salt movement and may reach dips up to 80-85° at the contact with the salt body. Commercial
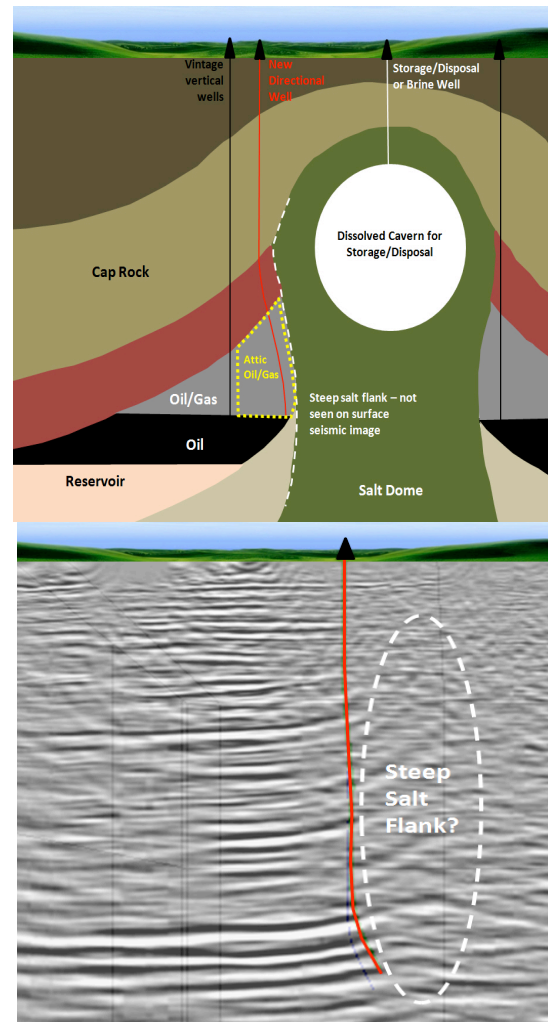

Figure 1: On the top we show a typical piercement dome. Vertical wells drain some of the trapped hydrocarbons but often 'attic oil' remains against the flank and is drained with directional wells, if the salt flank position can be determined. Knowledge of the outer limits of the dome is also required for safe cavern construction for strategic storage or brine production. On the bottom we show a line through the 3D seismic survey covering the Midway dome, courtesy of CGG. Whilst sub-horizontal sediments are clearly seen, the salt flank is not imaged with the surface seismic technique.

hydrocarbon accumulations have been found in the cap rock of salt domes as in the famous case at Spindletop (Gillespie, 1995) but as the cartoon indicates, and now documented by many commercial finds, more hydrocarbon is to be expected along the flanks of the dome at greater depths. Exploring for such traps has been hampered by the inability of the surface seismic method to image steeply dipping boundaries.

On the bottom of figure 1 is a line from a 3D surface seismic volume covering the Midway Dome in Mississippi, USA. One can clearly see sub-horizontal sediments and drag features up against the salt dome, but the steep flank of the salt dome is not visible. The well shown in the figure penetrates salt and the salt body is somewhere to the right of the well. The objective of this study was to image and locate the salt flank in order to reduce drilling risk and improve the seismic imaging.

Previous work shows how borehole seismic array tools have been used to position discrete points in 3D space that are related to the salt flank position in what is known as a salt proximity survey (SP) (Lou et al., 2012). We present a new and alternative method that creates a continuous salt flank image in 3D, and at high resolution, that is not prone to the errors associated with the Salt Proximity (SP) survey (Li et al., 2003).

By deploying three-component (3C) geophones inside the borehole we can record direct arrivals, refractions, reflections and diffractions of the wave field as it propagates away from the source and use this information to construct an accurate image in 3D of the salt flank.

Imaging Salt with VSP Data

A surface source, such as airgun or a seismic vibrator, generates seismic waves propagating in all directions. With the receiver outside and along the salt/sediment interface, in a general sense, we use the wave equation to forward propagate the source wave field through a model of the shallow sediments and salt body (Claerbout, 1985). Similarly - in a time-reversed mode - we reverse propagate the complete, recorded vector wave field from the receivers towards the salt body at local sediment velocities. Using an appropriate imaging condition (e.g. correlation), we are able to reconstruct the 3D salt sediment interface at a high degree of accuracy. The reconstructed interface is continuous and three-dimensional. The vector components of the full waveform data recorded at each 3C receiver are used and supply directional information of the incoming energy. This information may also be used for the orientation of the receiver tools, and we will therefore not require any pre-existing information with regards to orientation of the 3C geophones.

Treating the 3C data as a representation of a vector wave field, we create an image with a finite aperture both in plan view and in side view. If the surface source is too close to the edge of the salt, the horizontal aperture will narrow significantly. This is the case for Midway Dome, where the access was limited by the extent of the operator lease. A similar aperture-limiting effect occurs when the monitor well is close to the salt flank.

The final output is a cube of data at depth with a continuous and finely detailed salt interface in 3D. This image cube may best be viewed and interpreted using a computer vizualizer.

A General Approach

The velocity model is updated through an analytical process until the image gets sharp and well defined. Unlike traditional SP methods, the solution is unique and can be sharpened to give higher resolution through thousands of computer controlled iterative velocity updates. The top salt position needs to be known in order to construct a reliable image of the flank.

With the source on the surface and a standard three-component VSP array, we are able to image the flank of the Midway Dome in 3D, using this full-waveform, vector-based, two-way reverse-time migration.

A Ray-based Approach

As an alternative to the general full reverse-time approach, we have developed a significantly faster ray-based version, where – as with the general method - the source-side forward-projection and the receiver-side back-projection are performed in two separate velocity models, assuming that we don't know where the interface between the salt and the sediments are.

The two basic processes for generating images from the zero-offset and offset VSP data are deconvolution and migration: Simply put, migration transforms the map of reflection times to a volumetric map of formation properties. Deconvolution relates the seismic field generated by the source to the scattered or refracted field recorded by the receivers. In the process, the deconvolution process compresses the signal of the seismic source to a spike. The deconvolution is part of the imaging condition for migration and should properly be done inside the kernel of the migration, it is commonly assumed that the processes of migration (the propagation of the observed wave fronts into the formation) and the deconvolution (the collapsing of the source signature into a band-limited spike) can be factored out, such that the deconvolution can be done before the wave-field migration. However, analyzing the imaging process as an inverse scattering problem, Haldorsen (2002) and Haldorsen et al. (2013) show how the deconvolution should be done as part of the migration process. For each point in image space, combining the wave-field polarization measured by the 3C receiver, with the space-time relationship offered by the wave equation, we have generated complete estimates of both the source field and the scattered fields over a reasonably large section of space surrounding the data acquisition site. Deconvolving the "scattered" wave field by the "source"

wave field is the conditioning that converts the map of scattering times to a map of changes in acoustic impedance, the seismic image.
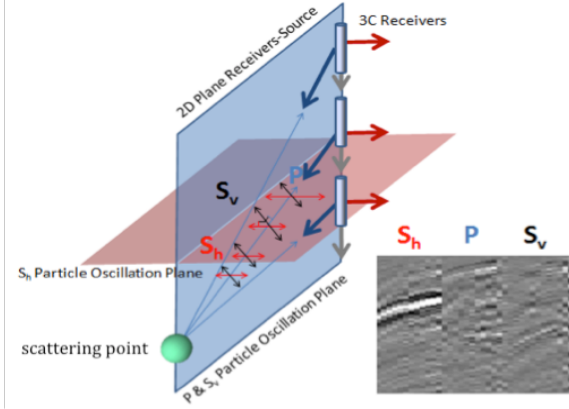

Figure 2: The elastic, scattered wave field seen by the 3C receivers.

As an illustration, in Figure 2 we show schematically the elastic components of the scattered wave field as recorded by the 3C receivers in a VSP tool. The compressional component (P), and the vertical shear (S_v) and horizontal shear (S_h), scattered at a point $\mathbf{x}_s$, and recorded a time $t_n(\mathbf{x}_s,\mathbf{x}_n)$ later at receiver n at location $\mathbf{x}_n$. These wave fields can be written as:

$$f_n^P(\omega;\mathbf{x}_s)\, e^{-i\omega t^P(\mathbf{x}_n,\mathbf{x}_s)} = \mathbf{p}^P(\mathbf{x}_n)\bullet\mathbf{d}(\mathbf{x}_n,\omega)$$

$$f_n^{Sv}(\omega;\mathbf{x}_s)\, e^{-i\omega t^{Sv}(\mathbf{x}_n,\mathbf{x}_s)} = [\mathbf{p}^{Sv}(\mathbf{x}_n)\times\mathbf{d}(\mathbf{x}_n,\omega)]_T$$

$$f_n^{Sh}(\omega;\mathbf{x}_s)\, e^{-i\omega t^{Sh}(\mathbf{x}_n,\mathbf{x}_s)} = [\mathbf{p}^{Sh}(\mathbf{x}_n)\times\mathbf{d}(\mathbf{x}_n,\omega)]_V$$

Here the vector $\mathbf{d}$ is the data vector, the vector $\mathbf{p}$ is the ray vector pointing in the direction of propagation for the different elastic wave-field components. The suffix T indicates a transverse component, and the suffix V indicates the component in the sagittal plane. The scattered P is polarized along the ray vector, the scattered S_v and S_h are polarized perpendicular to the ray - and all are (mostly) mutually orthogonal.

The ray-based process is essentially a 3-stage process where we for any point $\mathbf{x}_s$ in image space:

1) propagate the source function $f^P(\omega,\mathbf{x}_0)$ forward through the source-side velocity model from the source location $\mathbf{x}_0$ to the scattering point $\mathbf{x}_s$ (for economy of arguments, we are replacing the Green's function for wave-field propagation by a time delay operator):

$$f^{Ps}(\omega;\mathbf{x}_s) =\ f^P(\omega,\mathbf{x}_0)\, e^{-i\omega t^s(\mathbf{x}_s,\mathbf{x}_0)}$$

2) propagate the P projection of the recorded signal backwards through the receiver-side velocity model from each receiver n located at $\mathbf{x}_n$ to the scattering point $\mathbf{x}_s$ (again replacing the Green's function by a time-shift operator):

$$f_n^{Pr}(\omega;\mathbf{x}_s) =\ \mathbf{p}^r(\mathbf{x}_n)\bullet\mathbf{d}(\omega,\mathbf{x}_n)\, e^{i\omega t^r(\mathbf{x}_n,\mathbf{x}_s)}$$

3) correlate the two wave-field reconstruction in order to impose synchronicity and coherency at point $\mathbf{x}_s$ of the source-side and receiver-side estimates (i.e., $f^{Ps}(\omega;\mathbf{x}_s)$ and $f_n^{Pr}(\omega;\mathbf{x}_s)$), apply inverse Fourier transform, keeping only the $t=0$ values (i.e., sum over ω), sum over all receivers:

$$I(x,y) = \sum_n\sum_\omega f^{*Ps}(\omega;x,y)\, f_n^{Pr}(\omega;x,y)$$

Substituting, and re-arranging terms:

$$\begin{aligned}I(\mathbf{x}_s) &= \sum_n\sum_\omega f^{*Ps}(\omega;\mathbf{x}_s)\, f_n^{Pr}(\mathbf{x}_s)\\ &= \sum_n\sum_\omega f^{*P}(\omega)\, e^{i\omega t^s(\mathbf{x}_s,\mathbf{x}_0)}\,\mathbf{p}^r(\mathbf{x}_n)\bullet\mathbf{d}(\omega,\mathbf{x}_n)\, e^{i\omega t^r(\mathbf{x}_s,\mathbf{x}_n)}\\ &= \sum_n\sum_\omega\mathbf{p}^r(\mathbf{x}_n)\bullet\left[f^{*P}(\omega)\,\mathbf{d}(\omega,\mathbf{x}_n)\right]\, e^{i\omega[t^s(\mathbf{x}_s,\mathbf{x}_0)+t^r(\mathbf{x}_s,\mathbf{x}_n)]}\end{aligned}$$

This is a Kirchhoff style of migration sum of the correlation between the source wave field an the recorded data vector, projected on to the ray vector at the receiver, delayed by the total travel time from the source to the receiver and stacked over frequencies and receivers.

Following Haldorsen et al. (2013), for better resolution, we replace the correlation by an energy-weighted correlation, originating in the semblance-weighted deconvolution described by Haldorsen, Miller and Walsh (1994). This leaves:

$$I(\mathbf{x}_s) = \sum_n\sum_\omega\mathbf{p}(\mathbf{x}_n)\bullet\left[\frac{f^{*P}(\omega)}{E_n(\omega,\mathbf{x}_n)}\mathbf{d}(\omega,\mathbf{x}_n)\right]\, e^{i\omega[t^s(\mathbf{x}_s,\mathbf{x}_0)+t^r(\mathbf{x}_s,\mathbf{x}_n)]} \quad (1)$$

For economy of arguments, we have ignored the part of the Green's wave-field propagators that relate to amplitude alterations, such as absorption and spherical spreading. With the spherical spreading corrections added in, we will be using equation (1) for a fast, ray-based reverse-time imaging of the data acquired around the Midway Dome in Mississippi, USA.

Vector Migration, Zero-offset and Far-offset VSP

The ray-based process can be used with an appropriate velocity model to create images from both reflections and converted shear. This vector-based migration process uses travel times in combination with 3C, 3D polarization. The assumption that the compressional components are polarized perpendicular to the wave front and the shear components polarized tangentially to the wave front, allows an effective separation of compressional and shear contributions into two separate images.

Mississippi Case Study

The well is located on land in Mississippi, USA. The data were acquired in a deep well with a ten-level, three-component VSP array from 15,725 ft to mean sea level.

The three-component tools were separated by 50 ft cables. More than 250 levels were recorded for each source position. The seismic source was a 60,000 lb vibrator with a linear sweep from 4-130 Hz.

In addition to a "Salt Image" VSP, with rays penetrating through the salt, a zero-offset VSP and an offset VSP were also acquired with the objective to image more of the flank and the surrounding sediments, vey. Figure 3 shows the geometry of the well and the two shot points in relation to the assumed salt body.
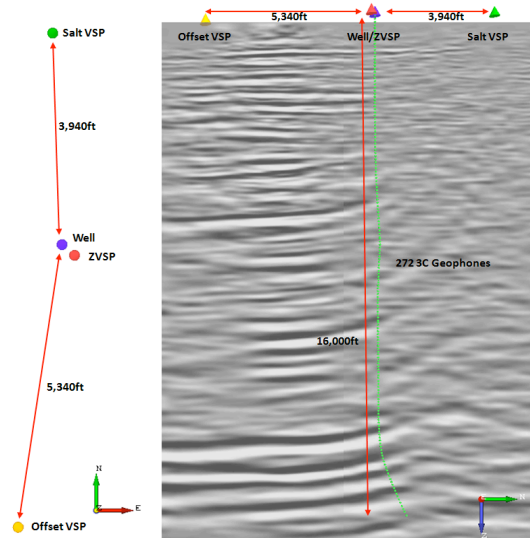

Figure 3: Plan and side view of the seismic source positions relative to the wellhead and with the assumed salt body to the right-hand side of the well. The seismic section is by courtesy of CGG.

Using the ray-based approach, we were able to create both compressional and converted shear images from the VSP data. From the zero-offset VSP data we could extend the image of the salt flank in the shallow section with the zero offset VSP dataset (Figure 4) and, using the offset VSP data, provide P-P and P-S images of the sediments, which juxtapose the salt body (Figure 5).

Once the salt-flank image has been constructed from the "Salt Image" VSP data using the general, full reverse-time method, a 3D image volume is saved for interpretation. In Figures 4 and 5 we show the image volume, clipped to show amplitudes at the salt flank only and loaded to a viewer. The 3D salt flank is shown in bright red. The original well and a sidetrack are shown with the geophones in pink. Both the original well and the sidetrack tagged salt and the locations of these points (indicated in green on Figures 4 and 5) confirm the accuracy of the imaging. The lateral distance between the well and the flank can be calculated at any point on the image.

In Figures 4 and 5, the graded, red-to-white background images are obtained by the much faster ray-based process.

The 3D salt flank image covers approximately 5000 ft vertical depth before the clear salt arrivals disappear on the raw recorded data. The offset VSP position was at a different orientation to the salt VSP but nevertheless the zero offset VSP and salt flank results have been rotated to look along the strike of the salt flank. The results of this operation are shown in Figure 4. The ray-based image from the zero-offset and offset VSP's clearly indicates that the salt flank continues upwards, appearing to slant away from the well. The image of the shallow section of the salt obtained by the fast, ray-based method thus complements the 3D image in the deeper section obtained by the vector, full reverse-time migration method. The total coverage exceeds 7500 ft.

When the 3D salt image is displayed with a surface-seismic cross line (in Figure 5), the salt-sediment boundary can clearly be seen. This also shows, quite dramatically, the absence of the significant steep interfaces on the surface-seismic image.

Figure 5 also shows comparisons of the surface seismic image with sedimentary reflected P and converted S images obtained by the ray-based images from the offset VSP data. In addition to the obvious improvement in resolution, the VSP results show clear evidence of uplifted sediments against the imaged salt flank. This provides a complete and accurate picture of the salt and sediment structure around the wells and zone of interest.

Conclusion

The deeper section of the salt flank has successfully been imaged in three dimensions using an approach based on full reverse-time migration. These images are complemented by images of the shallower part of the salt flank and of the sediments that juxtaposed the salt body - obtained by applying a fast, ray-based, reverse-time migration to data acquired in both zero-offset and offset VSP geometries.

The resulting images are used to enhance the processing and interpretation of the surface-seismic data and to reduce future drilling risk around the Midway Dome.

Acknowledgements

References

Claerbout, J. F., 1985, Imaging the Earth's Interior: Blackwell Science Inc.

Gillespie, R. H., 1995, Rise of the Texas oil industry: Part 1: Exploration at Spindletop: SEG The Leading Edge, Vol. 14, No. 1, pp. 22-24.

Haldorsen, J. B. U., 2002, Converted-shear and compressional images using Projection Imaging: The 64th EAGE Conference & Exhibition, Extended Abstracts, Paper F031.

Haldorsen, J. B. U., T. Hilton, M. Milenkovic, M. C. Schinelli, L. Furtado Soares, J. E. M. Lira, and A. Z. Nunes de Barrio, Formation Imaging from Three-Component Borehole-Seismic Data Using both Spacetime Relations and Wave-Field Polarization: 13th International Congress of the Brazilian Geophysical Society, Rio de Janeiro, Brazil, 2013.

Haldorsen, J., D. Miller, J. Walsh, 1994, "Multichannel Wiener Deconvolution of Vertical Seismic Profiles": Geophysics, **59**, No. 10, p. 1500-1511.

Li, Y., J. Jackson, S. Espinosa, and D. Faw, 2003, Uncertainties in mapping salt flanks with 3D salt proximity survey: SPE Annual Conference and Exhibition, SPE84574.

Lou, M., D. Cheng, and F. Doherty, 2012, 3D anisotropic calculation of salt-face exit point for VSP salt proximity surveys: SEG Technical Program Expanded Abstracts 2012: 1-5.
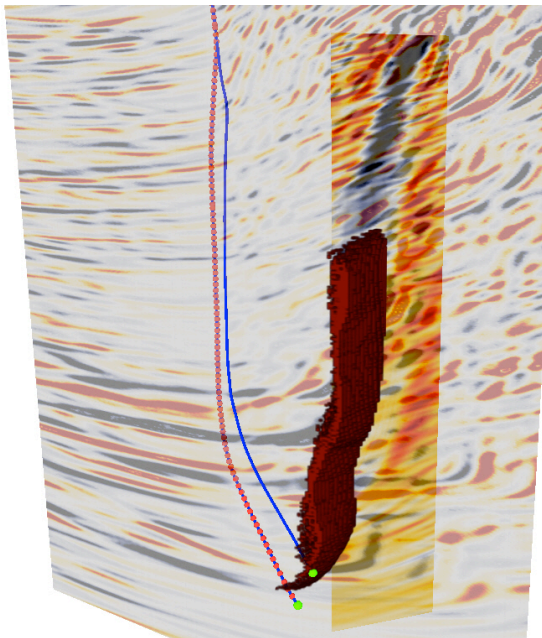

Figure 4: 3D salt flank image (red) displayed with the zero-offset VSP image showing a continuation of the salt flank in 2D in the shallow section. The back drop is the offset VSP P-P image showing the uplifted sediments agaist the salt dome. Salt entry points (green) and geophones (pink) are shown. Vertical coverage of flank is approximately 7750ft.
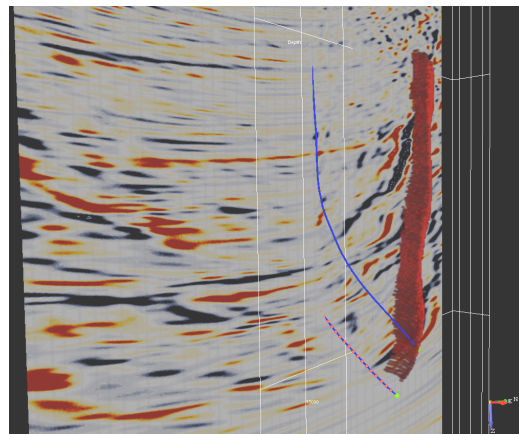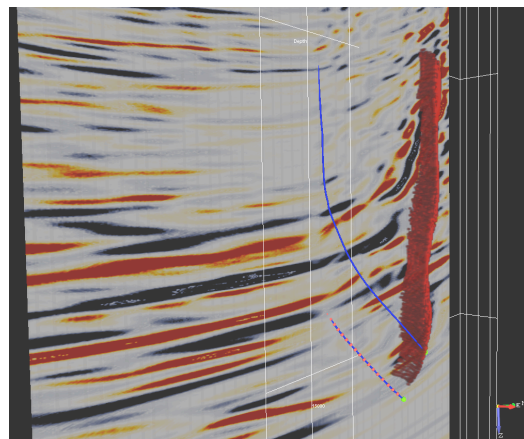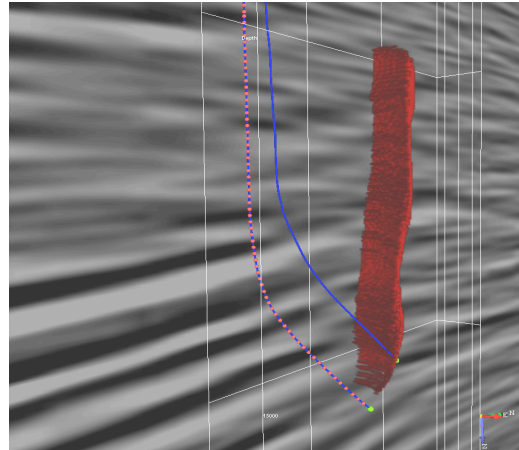

Figure 5: 3D salt flank image with surface seismic and VSP data. Surface seismic data (top), P-P offset VSP (middle), and P-S VSP image (bottom). The VSP images clearly show the uplifted sediments against the flank. First well, the sidetrack, salt entry points and geophone positions are shown.